JTTEES 5:483-489

Microstructural Examination of HVOF Chromium Carbide Coatings for High-Temperature Applications

J.M. Guilemany, J. Nutting, and N. Llorca-Isern

Chromium carbide/nickel chromium coatings obtained by the high-velocity oxyfuel thermal spray process were characterized using conventional and high-resolution microscopy to identify the complex microstructure that results from this thermal spraying technique. Thermal cycling and long isothermal treatment were studied, as were the adhesion properties of as-coated and thermally treated samples.

Keywords chromium carbide coatings, high-temperature applications, HVOF, microstructural characterization

1. Introduction

CHROMIUM carbide coatings are widely used in high-temperature wear-resistance applications in the aerospace, automotive, and transportation industries. Nickel chromium alloy generally serves as the metallic binder phase. Different compositions and microstructures of this cermet have been tested to identify optimum wear and corrosion properties, especially at high temperatures. The macroscopic behavior of the coatings usually depends on carbide grain size and shape, chemical composition, binder volume fraction, and the general morphology distribution (Ref 1-5).

The development of the high-velocity oxyfuel (HVOF) process for the production of sprayed coatings has required improved thermal spray powder characteristics in order to obtain high-quality coatings. The elevated temperatures in the combustion chamber, the chaotic and turbulent behavior inside the chamber, and the rapid heating and cooling of sprayed particles associated with the HVOF technique result in complex transformations of the initial phases during coating formation.

Different phases are present either as metallics or carbides in chromium carbide powders. Due to their low phase transformation temperatures (Ref 6), the stabilized phases present in the coating will be very similar for feedstocks of similar chemistry, even if the starting powder morphology is quite different.

The goals of the present work were to (1) characterize a commercially available powder based on Cr_3C_2 with a NiCr matrix, (2) study the optimal spraying parameters for coating production, and (3) characterize the as-sprayed coating before and after thermal cycling at 850 °C and long-term isothermal exposure at 650 °C.

Table 1 HVOF Spraying Parameters

Gas	J	N	D
$O_{2(SPLM)}$	462	420	378
$C_3H_{8(SPLM)}$	66	60	54
$N_{2(SPLM)}$	20	20	20

J.M. Guilemany, J. Nutting, and **N. Llorca-Isern,** University of Barcelona, Eng. Quimica-Metallurgia, Facultat Quimiques, Marti-Franques, 1, Barcelona 08028, Spain.

2. Experimental Procedure

A Plasma Technik CDS-100 (Sulzer-Metco, Wohlen, Switzerland) HVOF system was used. Spraying was performed under three different parameter sets (Table 1).

The powder and coating were characterized using different techniques. Powder particle size and particle size distribution were determined with the Microtrac X-100 (Leeds & Northrup, Sumney Town, PA, USA) laser analyzer. Powder flowability measurements were carried out in a Hall funnel according to ASTM B 213 (Ref 7). Density was measured using the AFNOR A-95-111-1977 method (Ref 8). The compositions of the particles forming the spray powders as well as the coating structure were determined in various ways. X-ray diffraction (XRD) for phase determination was carried out in a Siemens B-500 (Siemens Corporation, New York, NY) machine using Cu-Kα radiation at 40 kV and 20 mA. The patterns were used to identify the major phases present by comparison with the Joint Committee of Powder Diffraction Standards files. Scanning electron microscopy (SEM) (SS60, International Scientific Instruments, Inc., Suffolk, UK) and transmission electron microscopy (TEM) (Hitachi 800 TEM-STEM, Hitachi Scientific Instruments, Tokyo, Japan, and Philips 300kV, Philips Electronic Instruments Co., Mahwah, NJ, USA) were used to examine the microstructures of feedstocks and coatings. Electron probe microanalysis (EPMA) (Camebax 50; Cameca SX50, Courbevoie, France) was used to determine quantitatively the amount of carbon present in the various carbide phases and in the NiCr matrix. The instrument was operated at 6 kV for carbon determination and at 15 kV for nickel and chromium determination, with a spot size of less than 0.5 μm used for both purposes. An Inconel 600 standard for nickel and a Cr_3C_2 standard for carbon and chromium were used for comparison purposes; Pichou and Pichoir (PAP) method corrections were applied.

A 34Cr-4Mo carbon steel substrate was used. The surface was blasted at an air pressure of 3 to 4 bar with 30-mesh white alumina grit according to conditions published elsewhere (Ref 9). Coating hardness was determined by Vickers hardness (1 kg) and microhardness (100 g) techniques, and adhesion was meas-

ured using the ASTM C 633 test (Ref 10). The coating was submitted to two different thermal treatments. In the first method, test specimens were held in the furnace at 850 °C for 20 min and quenched; this cycle was repeated until the coating spalled. Spalling resistance of the coating was measured from the number of heating cycles required. In the second method, specimens were isothermally treated at 650 °C to study the oxidation resistance of the coating after a long thermal treatment. The same characterization techniques used on the as-sprayed coatings were used for the heat-treated samples.

3. Results

3.1 *Powder*

The laser diffraction particle size distribution of the starting powder corresponding to an average size of 45 μm is shown in Fig. 1. The feedstock exhibited a flowability of 28 s/50 g and a density of 3.75 g/cm^3. Examination of the starting powder by SEM revealed a spherical morphology (Fig. 2), with some particles having a relatively smooth, dense surface and others exhibiting rough surfaces. These differences correspond to different carbide distributions inside the particles (Ref 11). The powders are obtained by spray drying and are densified through a plasma operation, which leads to a multiphase system. X-ray diffraction pattern peaks were identified as Cr_3C_2, Cr_7C_3, $Cr_{23}C_6$, and a nickel-rich phase (Fig. 3a). A peak corresponding to $2\theta = 43.6$ ($d = 2.07$ Å) could not be identified. This peak might be Cr_3C, which is known to form in chromium-containing steels under rapid cooling rates, such as those experienced in welding. An SEM cross-section micrograph of the powder is shown in Fig. 4. Different levels of gray contrast are visible, suggesting variations in chemical composition in relation to the metallic element content. The phases present are Cr_3C_2, marked A; M_7C_3, marked B (where M = Cr + Ni); and $M_{23}C_6$, marked C. The NiCr metallic phase corresponds to the white phase in the micrograph. Quantitative measurements for the metallic phase are extremely difficult due to their small size with respect to the wavelength-dispersive spectrometry (WDS) spot size.

3.2 *Coating*

For the three spraying conditions applied to the substrate, no differences were apparent in the types of phases obtained or their distributions. X-ray diffraction of the coatings (Fig. 3b) revealed that the phases in the powder were also present in the coating; however, the peak intensities had changed slightly. An increase of $M_{23}C_6$ resulting from the transformation of Cr_3C_2 was suggested. Also present were Cr_2O_3 and NiO. The SEM micrograph of the coating shown in Fig. 5 identifies the various phases.

Quantitative compositional measurements were carried out using WDS-EPMA (Table 2). The nickel-rich phase in the coating had a composition different from that formed in the powder, resulting from the dissolution of chromium carbides in the liquid metallic phase (the nickel-rich phase) during the spraying process. Since the temperature in the HVOF flame can reach 2600 °C (Ref 12), dissolution might occur. It was also ap-

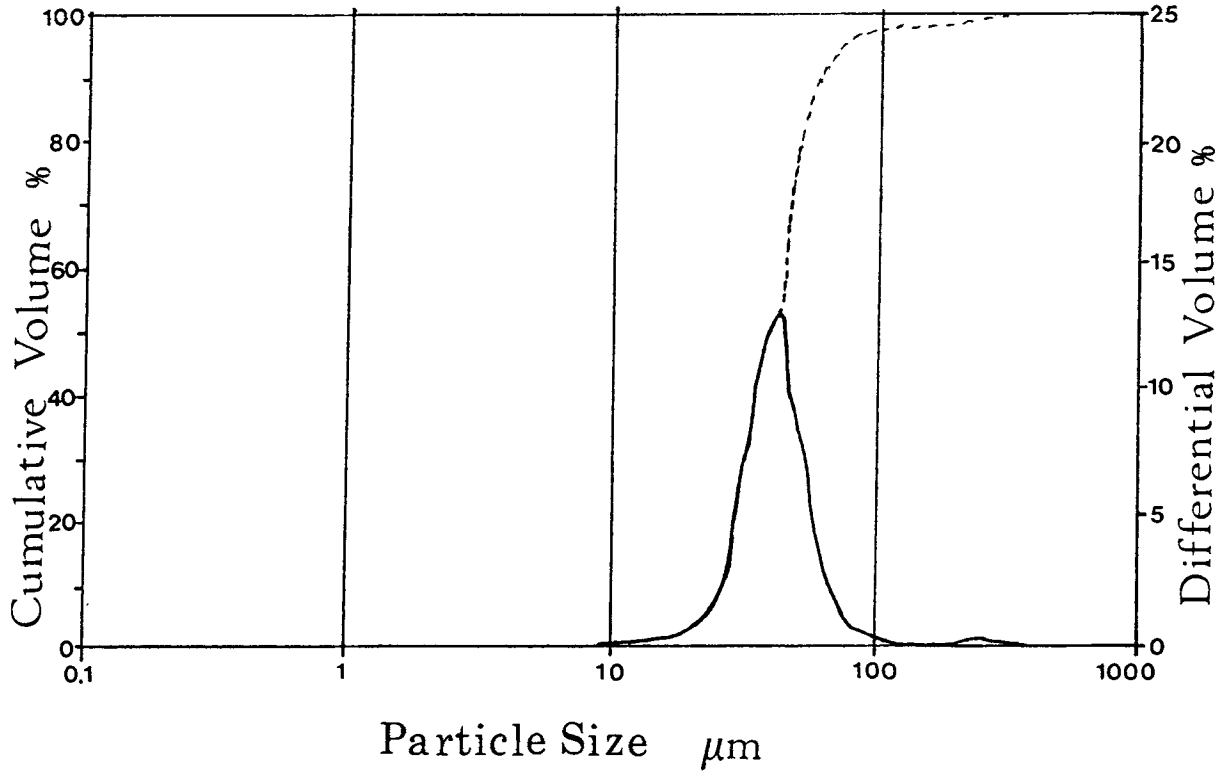

Fig. 1 Laser particle size analysis of the powder

parent that the metallic matrix phase composition varied across different regions.

The oxide phase was a mixture of NiO and Cr_2O_3, but XRD did not indicate the presence of a spinel. In some areas the microanalysis suggested the presence of Cr_3C (as was believed to be the case in the powder); again, the rapid cooling rates in the coating could favor the formation of this carbide.

For the interface and adjacent areas, thin-foil samples of the coating and substrate using the sandwich cross-section method were prepared for TEM examination. The substrate had a structure of ferrite and pearlite. The examination area in the different foils was about 100 μm from the interface. Moving toward the interface, the lamellae of the pearlite were spheroidized (Fig. 6), and eventually a martensitic structure was found (Fig. 7). This indicated that austenite had formed, transforming to martensite upon rapid cooling probably after the first layer was sprayed. No

Table 2 Chemical Composition determined by EPMA-WDS

Material	Composition, at.% C	Cr	Ni
Powder			
Cr_3C_2	40.1	59.9	...
M_7C_3	35.0	48.7	16.3
$M_{23}C_6$	20.9	57.8	21.3
Ni(Cr,C)	Undetermined	31.0	69.0
Coating			
Cr_3C_2	39.46	60.6	...
Ni(Cr,C)	32.0-23.0	53.0-36.0	14.0-40.0

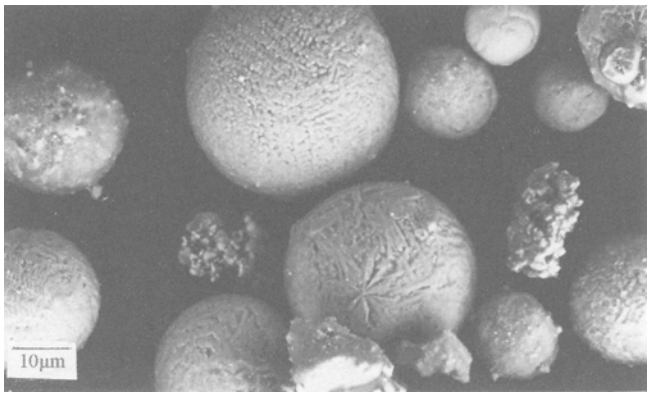

Fig. 2 SEM image of Cr_3C_2-NiCr powder

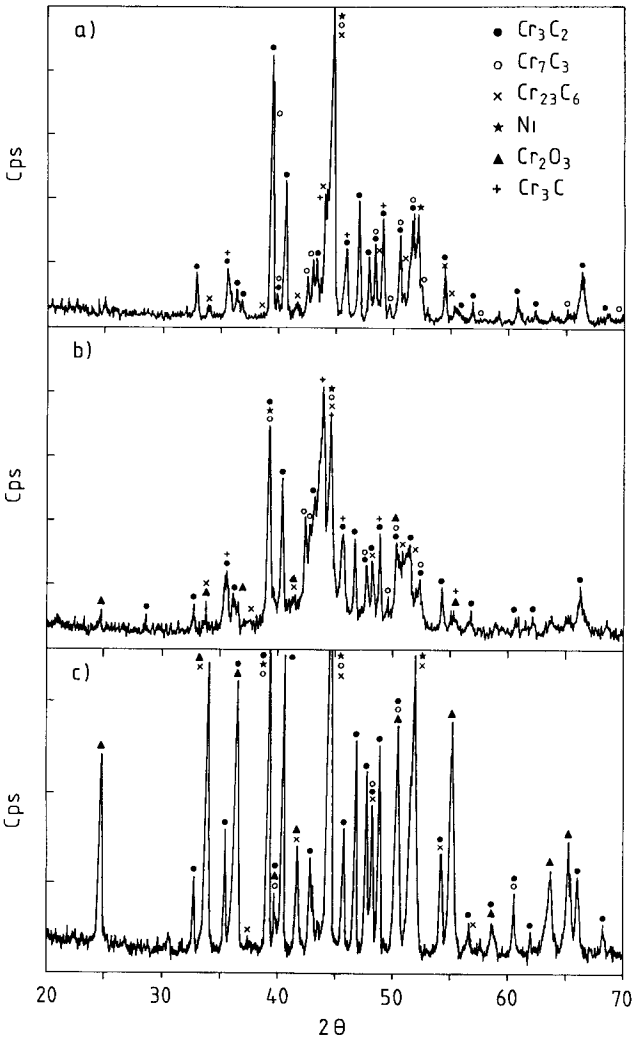

Fig. 3 XRD patterns of Cr_3C_2-NiCr. (a) Powder. (b) Coating. (c) Coating after thermal treatment

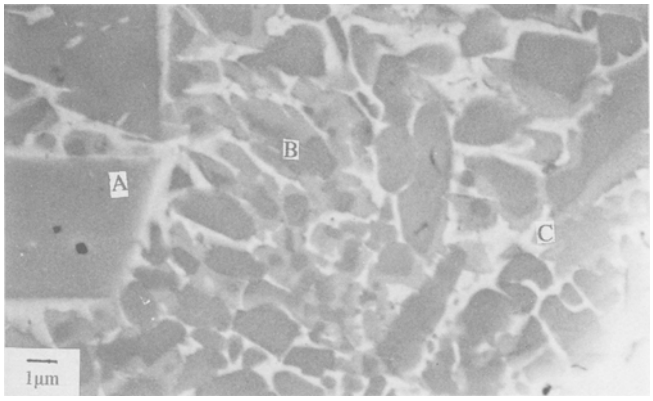

Fig. 4 Backscattered electron SEM image of powder cross section. A, Cr_3C_2; B, M_7C_3; C, $M_{23}C_6$

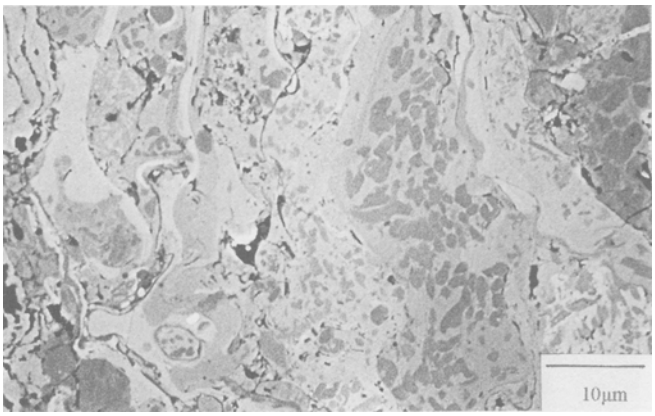

Fig. 5 Backscattered electron SEM image of Cr_3C_2-NiCr HVOF coating (cross section)

signs of substrate melting were observed, suggesting that the temperature was lower than 1465 °C (Ref 13). At the interface were very fine crystals with a body-centered cubic structure. The coating showed amorphous areas in the first layer (Fig. 8).

The metallic phase of the coating also exhibited a microcrystalline structure adjacent to the interface that extended into the coating away from the interface, with a grain size of about 50 nm. Dislocation shells were observed throughout (Fig. 9). Electron diffraction patterns from the other phases present in the coating indicated the existence of $Cr_{23}C_6$ and Cr_3C_2 (Fig. 10). The chromium carbide $Cr_{23}C_6$ is not well identified in the literature as a phase present in chromium carbide coatings. In our experiments, both XRD and TEM-electron diffraction confirmed the existence of this carbide in the starting powder, which increased in quantity after spraying. The structure also contained Cr_7C_3, as was confirmed by XRD.

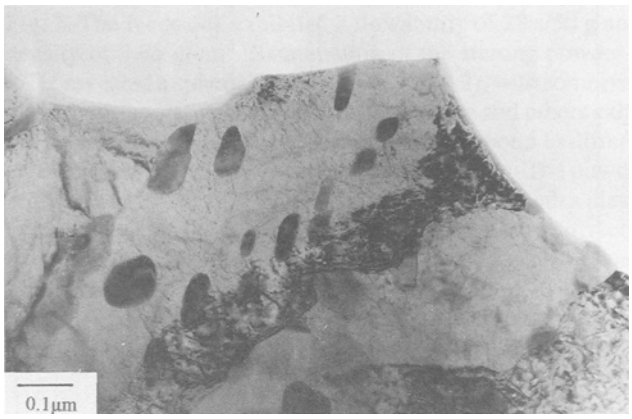

Fig. 6 TEM image of partially dissolved carbides in the substrate after spraying

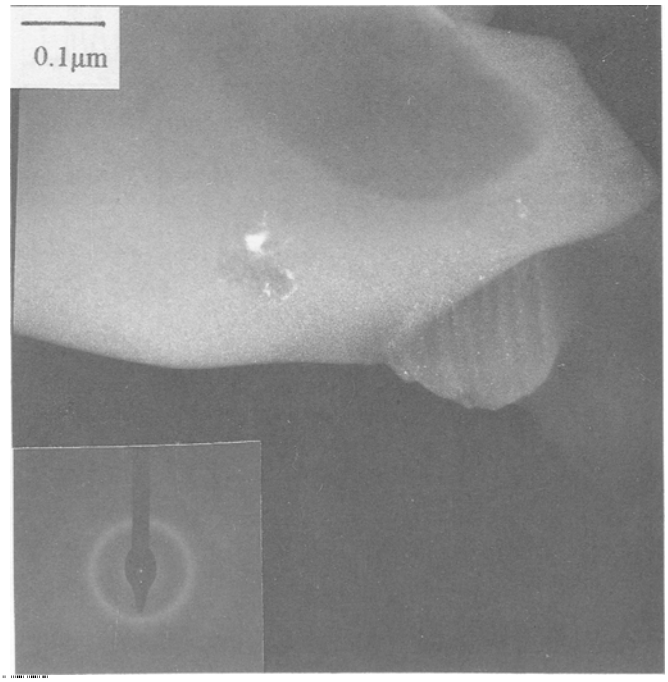

Fig. 8 TEM dark-field image of amorphous area in the coating

The adhesion strength of Cr_3C_2-NiCr coatings on the steel was measured using the ASTM C 633 test method. Failure occurred at the adhesive at a value of 85 MPa for the as-coated specimen (Table 3).

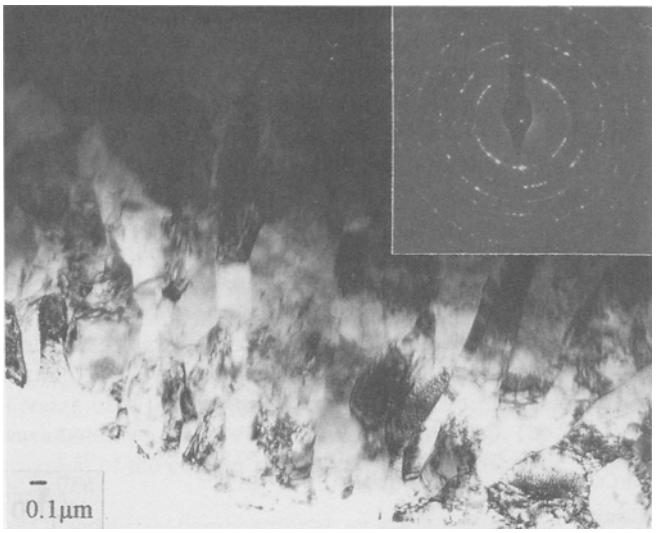

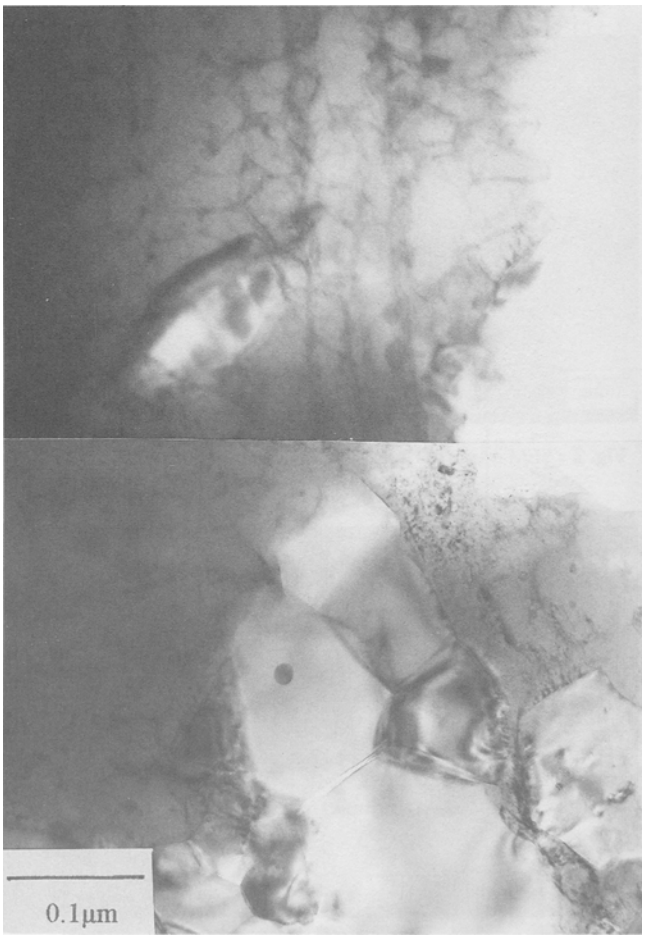

Fig. 9 TEM image of the coating containing dislocation shells

Chromium carbide coatings are used primarily in elevated-temperature applications. Tests were carried out on the coated samples to assess their thermal shock resistance and thermal stability. The method for determining thermal shock resistance was based on the work of Takeuchi et al. (Ref 14). The adhesion results obtained are presented in Table 3. The coatings produced under high- and medium-energy flame conditions (Table 1) showed cracks after only three thermal cycles, whereas coatings produced using low-energy spraying parameters required 11 cycles before cracks appeared. X-ray diffraction patterns obtained after different thermal cycles showed that the intensity of the chromium oxide peaks increased and that the Cr_3C peak disappeared (Fig. 3c), possibly because of an in situ transformation of the Cr_3C to Cr_3C_2. Examination of the coating revealed the presence of complex Fe-Ni-Cr oxides, suggesting that iron had diffused into the coating during thermal cycling. Figure 11 corresponds to a sample thermally cycled for nine cycles (850 °C + quenching) and then tested according to ASTM C 633 (adhesion test value of 52 MPa). Similarly, the peak intensities of the other carbides present in the coating also changed, indicating that carbide decomposition occurred with the metallic elements going into the matrix. If we consider the metallic phase as a Ni-Cr-C system, thermal treatment following a precipitation mechanism leads to the formation of carbides.

Adhesion tests on specimens after three thermal cycles (before cracks formed in the high- and medium-energy deposits) gave strengths of 52 MPa; a similar value was obtained for the low-energy deposit after nine cycles. The results indicate that even a few thermal cycles can lower the adhesive strength.

Isothermal treatment of the coatings at 650 °C for 283 h also produced changes in coating structure. There was a significant decrease in the adhesive strength of the coating to 17.5 MPa; such a change is probably due to carbide precipitation at the interface. Images produced by TEM revealed both intragranular and intergranular precipitation of small particles of Cr_3C_2, as confirmed by XRD, in the metallic phase (Fig. 12).

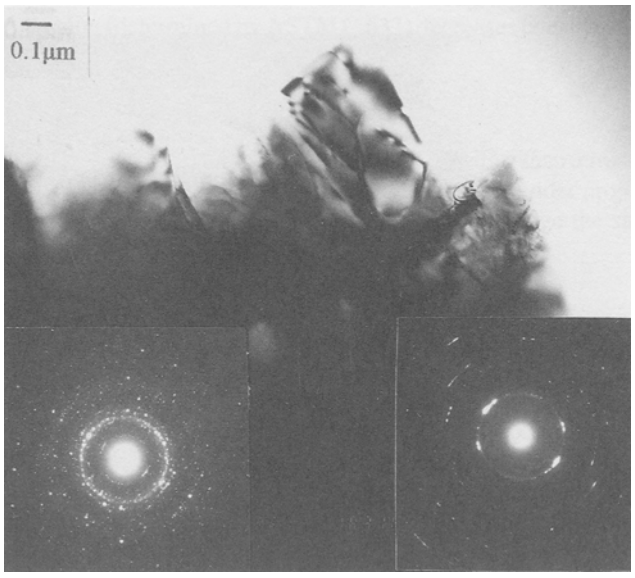

Fig. 10 TEM image of coating. Electron diffraction patterns: left, $Cr_{23}C_6$; right, Cr_3C_2

4. Discussion

During the manufacture of powders for thermal spraying, compositional variations are established that can then influence the composition in different regions of the as-deposited coatings. Thus, if the metallic phase in the powder has a low carbon content, then the carbides dissolve during spraying and increase the carbon and alloy content of the metallic matrix. However, the initial carbides present are not changed in type, although their volume fraction and general morphology in the coatings can be changed. As a result of the atmospheric spraying process, oxidation can occur and produce metallic oxides, which are incorporated in the coating as small lamellae.

Table 3 Results of adhesion test (ASTM C 633)

Condition	Failure value, MPa
As coated	>85
Thermal treatment: 9 cycles (850 °C + quench)	52.30
Isothermal treatment: 285 h at 650 °C	17.50

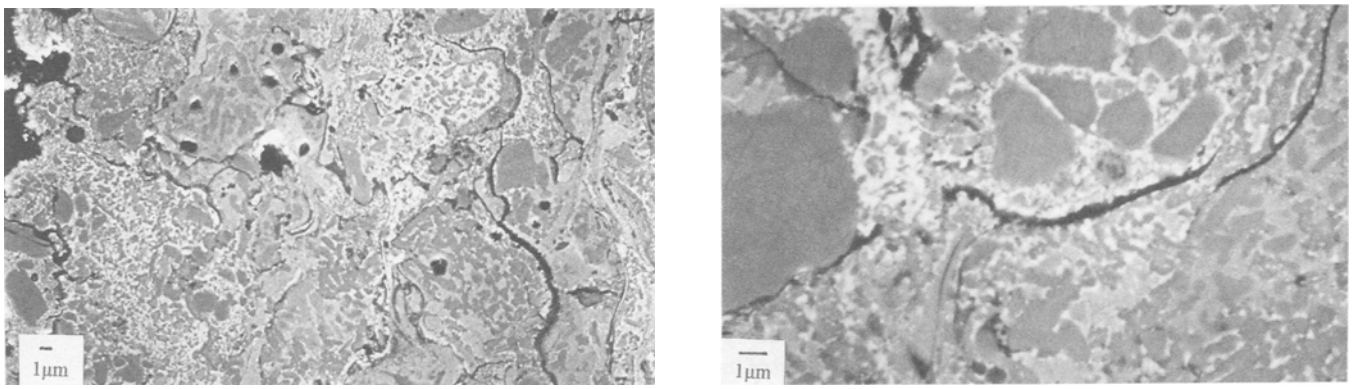

(a) (b)

Fig. 11 (a) Backscattered electron SEM image of thermally treated sample after 9 cycles (850 °C + quenching) Coating had been stripped from substrate following adhesion testing. (b) Detail of the microstructure

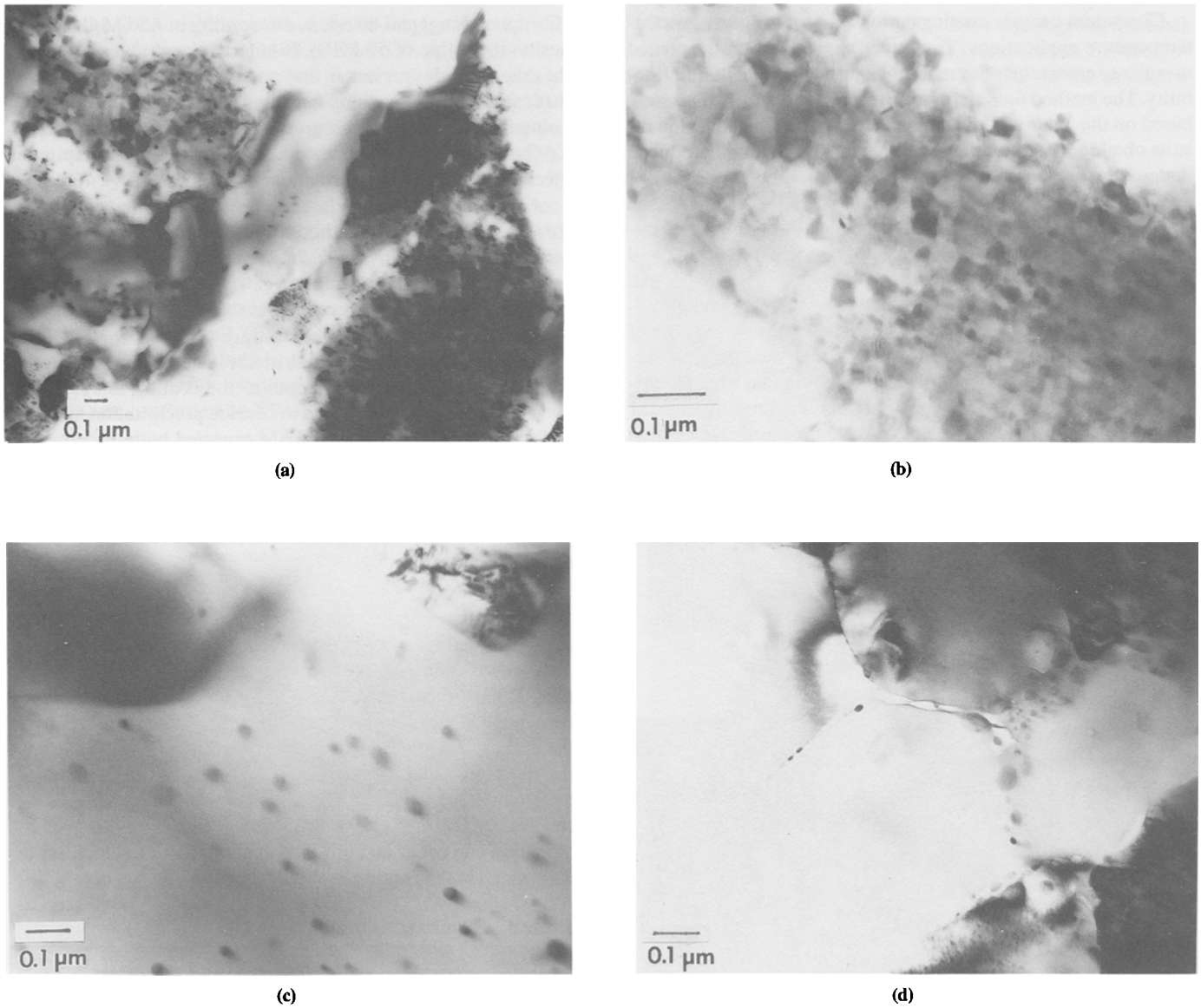

Fig. 12 TEM image of a coating after isothermal treatment at 650 °C for 265 h. (a) General. (b) Small crystals. (c) Intragranular precipitation. (d) Intergranular precipitation

When the particles strike the substrate, the metallic phase is liquid. However, due to the thermal properties of the substrate and particle components, rapid cooling occurs; it appears that the temperature at the interface between the substrate and the coating is insufficient to completely melt the substrate. The microstructural evidence suggests that neither solid-state diffusion nor substrate melting occurs. In the substrate, behind the interface, the temperature is high enough to dissolve the cementite particles from the pearlite and for austenite to form. During subsequent rapid cooling, this austenite transforms to martensite. Farther into the substrate, where complete transformation to austenite has not occurred, there is partial spheroidization of the cementite, indicating a long soaking time at a temperature below the eutectoid temperature. Changes in the substrate near the coating can promote residual stresses that decrease coating service life.

As the coating is built up, carbides and oxides enhance its thermal resistance, producing a local thermal treatment that causes recrystallization away from the interface. This is confirmed by the absence of amorphous areas inside the bulk coating and a significant amount of small crystals.

The adhesion test was performed for the purpose of comparison by applying uniaxial tensile load. The results indicate that thermal cycling decreases coating-substrate adhesion, even if the resulting values are relatively high.

5. Conclusions

For Cr_3C_2-NiCr feedstocks of similar chemistry, the stabilized phases in the coating obtained by a HVOF process are similar. The NiCr metallic phase can form a solid solution with

carbides, and thus its chemical composition varies throughout the coating.

The temperature achieved by the substrate at the interface when coating with Cr_3C_2-NiCr by the HVOF process is not high enough to melt the steel substrate. The thermal conditions of the process promote austenitization near the interface. The austenite transforms to martensite, and no further heating sources (i.e., new sprayed layers) cause tempering. However, behind the interface where no austenitization has taken place, further spraying promotes the thermal conditions required for partial dissolution of cementite. The microstructural changes, especially those that can take place near the substrate-coating interface, can contribute to the residual stresses of the system.

Metastable Cr_3C carbide, resulting from a rapid cooling process, is found in the coating but disappears after thermal treatment. Thermal treatment produces complex Fe-Ni-Cr oxides, suggesting that iron diffuses into the coating and that carbide decomposition occurs. The metallic phase of Ni-Cr-C chemistry incurs a precipitation transformation that results in the formation of both intergranular and intragranular carbides. Adhesion (determined by ASTM C 633) decreases considerably after thermal treatments.

Acknowledgments

The authors would like to thank the Comisión Interministerial de Ciencia y Tecnologia for financial support under project MAT 94-0013. J. Nutting would like to acknowledge the sabbatical concession SAB 930020.

References

1. J.M. Houben, Future Development in Thermal Spraying, Thermal Spray Coatings—New Materials, Processes and Applications, F.N. Longo, Ed., American Society for Metals, 1984, p 1-19
2. M. Smith, W. Oberkaupf, K. Kowalsky, and D. Marantz, HVOF: Particle Flame Diagnostics and Coating Characteristics, *Thermal Spray Research and Applications,* T.F. Bernecki, Ed., ASM International, 1991, p 587-592
3. M.L. Thorpe and H.J. Richter, A Pragmatic Analysis and Comparison of HVOF Processes, *J. Therm. Spray Technol.,* Vol 1 (No. 2), 1992, p 161-170
4. S.V. Joshi, Comparison of Particle Heat-up and Acceleration during Plasma and High Velocity Oxy-fuel Spraying, *Powder Metall. Int.,* Vol 6, 1992, p 373-380
5. M. Vardelle, A. Vardelle, A.C. Léger, and P. Fauchais, Dynamics of Splat Formation and Solidification in Thermal Spraying Processes, *Thermal Spray Industrial Applications,* C.C. Berndt and S. Sampath, Ed., ASM International, 1994, p 555-562
6. *Alloy Phase Diagrams,* Vol 3, *ASM Handbook,* ASM International, 1992, section 2
7. "Standard Test Method for Flowability of Powders," B 213, *Annual Book of ASTM Standards,* ASTM, 1982
8. "Determination of Apparent Density by Funnel Method," A-95-111-1977, *Recueil de normes françaises AFNOR, Métallurgie des poudres,* 2nd ed., Association Française de Normalisation, Paris, 1981 (in French)
9. J.M. Guilemany, N. Llorca-Isern, and P.J. Szabó, Study of Residual Stress in Surface Preparation for Thermal Spray Processes, *Euromat '94 Proc.,* Hungary, Societe Française de Metallurgie et de Materiaux, 1994, p 837-840
10. "Standard Test Method for Adhesion or Cohesive Strength of Flame-Sprayed Coatings," C 633-79, *Annual Book of ASTM Standards,* Part 17, ASTM, 1982, p 636-642
11. J.M. Guilemany, J. Nutting, and N. Llorca-Isern, Characterisation of Cr_3C_2-NiCr Cermet Powder for High Velocity Oxyfuel Spraying, *Powder Metall.,* Vol 37 (No. 4), 1994, p 289-292
12. "Introduction to CDS," Report, Plasma Technik AG, Wohlen, Switzerland, 1990, p 1-12
13. R.R. Subramanian and D.E. Laughlin, in *Alloy Phase Diagrams,* Vol 3, *ASM Handbook,* ASM International, 1992, section 2
14. J. Takeuchi, A. Nakahira, and G. Barbézat, Cr_3C_2-NiCr Cermet Coatings Using Some HVOF, APS and VPS Processes, *Thermal Spraying Conf. Proc.,* Deutschen Verband für Schweisstechnik, Aachen, Germany, 1993, p 11-14